

Supporting Information

Highly efficient separation of C₂H₂ from CO₂ and C₂H₄ enabled by an anion-pillared metalloporphyrin MOF with sandwich-like binding sites

Miaoyu Liu^{†a}, Xiao-Wen Gu^{†b}, Chenyan Lin^a, Baixue Dong^a, Zhongjie He^a, Bo Xie^a,
Xu Zhang^c, Bin Li^b, Hui-Min Wen^{*a} and Jun Hu^a

[†] These authors contributed equally to this work.

^a College of Chemical Engineering, Zhejiang University of Technology, Hangzhou 310014, China. E-mail: huiminwen@zjut.edu.cn.

^b State Key Laboratory of Silicon and Advanced Semiconductor Materials, School of Materials Science and Engineering, Zhejiang University, Hangzhou 310027, China.

^c Jiangsu Engineering Laboratory for Environmental Functional Materials, School of Chemistry and Chemical Engineering, Huaiyin Normal University, Huaian, 223300, Jiangsu Province, China

Table of Contents

Supplementary Experimental Section

Supplementary Tables S1-S5

Supplementary Figures S1-S16

Supplementary References

Supplementary Experimental Section

1. General procedures and materials

All starting reagents and solvents were purchased from commercial companies and used without further purification. 5,10,15,20-Tetra(4-pyridyl)porphyrin-Cu(II) (Cu-TPyP) was simply synthesized through a one-step reaction procedure according to the literature.^[1] High-resolution mass spectra (HRMS) were recorded on Agilent 1290-6545XT. Powder X-ray diffraction (PXRD) patterns were measured by BRUKER D8 ADVANCE diffractometer employing Cu-K α radiation ($\lambda = 1.542 \text{ \AA}$) operated at 30 kV and 15 mA, scanning over the range 2–45° (2θ) at a rate of 2°/min. N₂ (99.99%), C₂H₂ (99.6%), C₂H₄ (99.99%), CO₂ (99.99%), He (99.999%), mixed gases of C₂H₂/C₂H₄ (1/99, v/v), and C₂H₂/CO₂ (50/50, v/v) mixtures were purchased from JinGong Company (China).

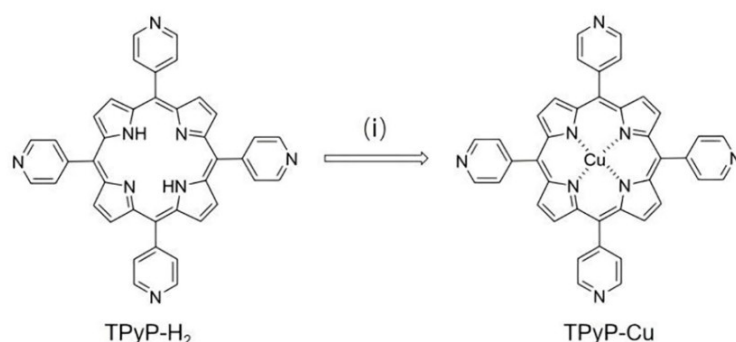
2. Powder X-ray Crystallography

Despite extensive attempts, single crystals of ZJUT-6 suitable for single-crystal X-ray diffraction studies were not synthesized successfully. Therefore, we relied on powder X-ray diffraction (PXRD) to confirm the high purity of the powder sample and to simulate the crystallographic structure of ZJUT-6.^[2] The PXRD measurements were performed on X'Pert PRO diffractometer, operated at 40 kV and 44 mA and CuK α radiation ($\lambda = 1.542 \text{ \AA}$). Data were collected in the 2θ range of 2–45° with a step size of 0.2° at room temperature. We first indexed the PXRD pattern and used a tetragonal *I4/mcm* space group to build the model of ZJUT-6. Then, based on the similar 4-connected framework of CPM-131,^[3] a structural model for ZJUT-6 was built. The unit cell parameters were determined to be $a = b = 19.9477 \text{ \AA}$ and $c = 13.8723 \text{ \AA}$. As shown in Figure S1, the simulated PXRD pattern of our structural model agrees excellently with experimental data, strongly supporting its validity. Some structural information of ZJUT-6 is given in Table S3.

3. Procedures for ligand synthesis

Scheme S1. The Synthetic route of Cu-TPyP metallic ligand. Reagents and conditions:

(i) $\text{Cu}(\text{OAc})_2 \cdot 2\text{H}_2\text{O}$, $\text{MeOH}/\text{CHCl}_3$, reflux, 12 hours.



Synthesis of 5,10,15,20-Tetrakis(4-pyridyl)porphyrin-Cu(II) (Cu-TPyP): TPyP-H₂ (0.62 g, 1.0 mmol) and $\text{Cu}(\text{OAc})_2 \cdot 4\text{H}_2\text{O}$ (2.49 g, 10 mmol) were dissolved into 100 mL CHCl_3 (mixed with 30 milliliters of CH_3OH), and then heat the mixture to reflux for 12 hours. After cooling to room temperature, the $\text{CHCl}_3/\text{CH}_3\text{OH}$ solvents were removed under reduced pressure. The obtained product was washed several times with water and methanol, and then Cu-TPyP was obtained after drying. HRMS (ESI) for $\text{C}_{40}\text{H}_{24}\text{CuN}_8$ $[\text{M}+\text{H}]^+$ m/z: calcd. 680.1420, found 680.1497.

4. Synthesis of $[\text{Cu}(\text{Cu-TPyP})(\text{SiF}_6)]_n$ (ZJUT-6)

0.075 mmol (51 mg) of 5,10,15,20-tetra(4-pyridyl)porphyrinato)copper(II) (Cu-TPyP) was sonicated in 3 ml of acetic acid to form solution A. 15 mmol (32 mg) of copper hexafluorosilicate (CuSiF_6) was dissolved in 2 ml of ethanol to form solution B. Then solution B was then slowly added to solution A while shaking, and placed the mixture in an oven at 70 °C for 12 hours. After the reaction was completed, the dark red powder was filtered and rinsed multiple times with anhydrous ethanol, obtaining the powder sample of ZJUT-6.

5. ICP-OES measurements

The ICP-OES test of ZJUT-6a was performed by Agilent 720ES with an RF power of 1.2KW and Plsama flow rate of 15.0 L/min. Samples should be subjected to appropriate digestion and dilution processes to ensure that they meet the analytical

requirements of the instrument.

6. Gas sorption measurements

Gas adsorption isotherms were measured by Micromeritics ASAP 2020 PLUS HD88. To remove all guest solvents from the framework, fresh powder samples were first subjected to at least eight solvent exchanges with dry ethanol over a period of three days. The solvent-exchanged samples were evacuated at room temperature (298 K) for 12 h, followed by an additional 12 h at 323 K until the outgassing rate prior to measurement was 5 mmHg min^{-1} . Adsorption measurements were performed in a liquid nitrogen bath at 77 K. Adsorption isotherm measurements were performed using an ice-water bath (slurry) and a water bath at 273 K and 296 K, respectively.

7. Breakthrough experiments

The breakthrough curves of ZJUT-6a were measured on a homemade apparatus for gases mixtures $\text{C}_2\text{H}_2/\text{C}_2\text{H}_4$ (1/99) and $\text{C}_2\text{H}_2/\text{CO}_2$ (50/50) at 298 K and 1.0 bar. In the separation experiment, ZJUT-6a particles with diameters of 200-300 μm were prepared and packed into $\Phi 4 \times 120$ mm stainless steel column, and the column was activated under reduced pressure at 323 K overnight. The experimental set-up consisted of two fixed-bed stainless steel reactors. One reactor was loaded with the adsorbent, while the other reactor was used as a blank control group to stabilize the gas flow. The gas flows were controlled at the inlet by a mass flow meter as 2 mL/min , and a gas chromatograph (TCD-Thermal Conductivity Detector, detection limit 0.1 ppm) continuously monitored the effluent gas from the adsorption bed. Prior to every breakthrough experiment, we activated the sample by flushing the adsorption bed with helium gas for 2 hours at 373 K. Subsequently, the column was allowed to equilibrate at the measurement rate before we switched the gas flow. After completing the breakthrough experiments, ZJUT-6a was activated by purging with a flow of helium gas (10 mL min^{-1}) for 2 hours at room temperature. Then, the activated samples were subjected to cyclic experiments.

8. Virial Graph Analysis

Estimation of the isosteric heats of gas adsorption (Q_{st}).

A virial-type expression of comprising the temperature-independent parameters a_i and b_j was employed to calculate the enthalpies of adsorption for C_2H_2 , C_2H_4 and CO_2 (at 273 K and 296 K) on ZJUT-6a. In each case, the data were fitted use equation:

$$\ln P = \ln N + 1/T \sum_{i=0}^m a_i N_i + \sum_{j=0}^n b_j N_j \quad (1)$$

Here, P is the pressure expressed in mmHg, N is the amount absorbed in mmol g^{-1} , T is the temperature in K, a_i and b_j are virial coefficients, and m , n represent the number of coefficients required to adequately describe the isotherms (m and n were gradually increased till the contribution of extra added a and b coefficients was deemed to be statistically insignificant towards the overall fit. And the average value of the squared deviations from the experimental values was minimized). The values of the virial coefficients a_0 through a_m were then used to calculate the isosteric heat of absorption using the following expression:

$$Q_{st} = -R \sum_{i=0}^m a_i N_i \quad (2)$$

Q_{st} is the coverage-dependent isosteric heat of adsorption and R is the universal gas constant. The heat enthalpy of C_2H_2 , C_2H_4 and CO_2 sorption for complex ZJUT-6a in this manuscript are determined by using the sorption data measured in the pressure range from 0-1 bar (at 273 K and 296 K).

9. Fitting of pure component isotherms

Experimental data on pure component isotherms for C_2H_2 , C_2H_4 and CO_2 in ZJUT-6a were measured at 296 and 273 K. The pure component isotherm data for C_2H_2 , C_2H_4 and CO_2 were fitted with the single-site Langmuir-Freundlich equation:

$$q = q_{sat} \frac{bp^v}{1 + bp^v} \quad (3)$$

with T -dependent parameter b

$$b_A = b_0 \exp\left(\frac{E}{RT}\right) \quad (4)$$

The parameters are provided in Table S4.

10. IAST calculations of adsorption selectivities

The selectivity of preferential adsorption of component 1 over component 2 in a mixture containing 1 and 2, can be formally defined as:

$$S_{ads} = \frac{q_1/q_2}{p_1/p_2} \quad (5)$$

In equation (5), q_1 and q_2 are the molar loadings of the adsorbed phase in equilibrium with the bulk gas phase with partial pressures p_1 and p_2 . We calculate the values of q_1 and q_2 using the Ideal Adsorbed Solution Theory (IAST).

11. GCMC simulations

All the GCMC simulations were carried out with the Sorption program (BIOVIA Material Studio 8.0) to investigate the interactions between the framework and gas molecules.^[4] The interaction energy between hydrocarbon molecules and framework were computed through the Coulomb and Lennard-Jones 6–12 (LJ) potentials. A cutoff radius of 12.5 Å was used to handle the nonbonding interactions, and the Ewald & Group summation method was applied to calculate the long-range electrostatic interactions. The simulations were carried out at 296 K, adopting the locate task, Metropolis method in Sorption module and a mixed set of UFF and DREIDING force field parameters were adopted to describe the LJ parameters for the atoms in framework, respectively. Each state point of GCMC simulations contained 1×10^7 steps to guarantee equilibration followed by 1×10^7 steps to sample the required thermodynamics properties. The crystal structures of ZJUT-6a were chosen for related simulations without further geometry optimization. The framework was considered to be rigid during the simulation. Partial charges for atoms of guest-free ZJUT-6a were derived from QEq method and QEq_neutral 1.0 parameter. For gas molecules, LJ

parameters for C₂H₂, CO₂ and C₂H₄ were taken from the united-atom TraPPE force field.

12. Gas equilibrium adsorption capacity and separation factor

The complete breakthrough of gas was indicated by the downstream gas composition reaching that of the feed gas. On the basis of the mass balance, the gas adsorption capacities can be determined as follows:

$$q_i = \frac{C_i V}{22.4 \times m} \times \int_0^t \left(1 - \frac{F}{F_0}\right) dt \quad (6)$$

Where q_i is the equilibrium adsorption capacity of gas i (mmol g⁻¹), C_i is the feed gas concentration, V is the volumetric feed flow rate (cm³ min⁻¹), t is the adsorption time (min), F_0 and F are the inlet and outlet gas molar flow rates, respectively, and m is the mass of the adsorbent (g). The separation factor (α) of the breakthrough experiment is determined as:

$$\alpha = \frac{q_A y_B}{q_B y_A} \quad (7)$$

in which y_i is the molar fraction of gas i ($i = A, B$) in the gas mixture.

Notation

q_i	Component molar loading of species i , mol kg ⁻¹
q_{sat}	Saturation loading, mol kg ⁻¹
b	Langmuir-Freundlich constant, kPa ^{-ν}
p_i	Partial pressure of species i in mixture, kPa
p_t	Total system pressure, kPa
T	Absolute temperature, K

Greek letters

ν	Freundlich exponent, dimensionless
-------	------------------------------------

Supplementary Tables

Table S1. Physicochemical properties of C₂H₂, C₂H₄ and CO₂ molecules.


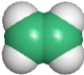
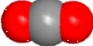
Gas molecule	C ₂ H ₂	C ₂ H ₄	CO ₂
Molecular model			
Kinetic diameter (Å)	3.3	4.2	3.3
Polarizability ($\times 10^{-25}$ cm ³)	39.3	42.5	29.11
Quadrupole moment ($\times 10^{-26}$ esu cm ²)	7.2	1.5	4.3

Table S2. The Cu contents of Cu-TPyP and ZJUT-6 measured by ICP-OES, indicating that the successful metallization of TPyP ligand. Note that the bias may originate from the presence of solvent molecules in the as-synthesized Cu-TPyP and ZJUT-6 sample.

Sample	Cu-TPyP	ZJUT-6
Cu (%)		
Theoretical value (wt%)	9.34	14.34
ICP-OES (wt%)	7.28	11.29

Table S3. Lattice parameters of the modeled structure of ZJUT-6.

Unit cell parameters	ZJUT-6
Formula	$C_{40}N_8H_{24}F_6Cu_2Si$
Formula weight	885.85
Crystal system	Tetragonal
Space group	<i>I4/mcm</i>
a (Å)	19.9477
b (Å)	19.9477
c (Å)	13.8723
α (°)	90
β (°)	90
γ (°)	90
Volume (Å ³)	5519.94
Z	4
D_{calcd} (g cm ⁻³)	1.06588

Table S4. Single-Langmuir-Freundlich parameter fits for C₂H₂, CO₂ and C₂H₄ in ZJUT-6a. The fits are based on experimental isotherm data at 296 K.

	q_{sat} mol kg ⁻¹	b_0 kPa ^{-ν}	ν dimensionless
C ₂ H ₂	11.62927	0.12028	0.38967
C ₂ H ₄	4.62569	0.05864	0.81646
CO ₂	5.93904	0.01897	0.98027

Table S5. Comparison of C₂H₂/CO₂ and C₂H₂/C₂H₄ selectivities for ZJUT-6a with some reported multipurpose materials.

Materials	C ₂ H ₂ uptake at 1 bar (mmol g ⁻¹) ^a	IAST selectivity		Q_{st}^b (kJ mol ⁻¹)	Ref.
		C ₂ H ₂ /CO ₂ (50/50, v/v)	C ₂ H ₂ /C ₂ H ₄ (1/99, v/v)	C ₂ H ₂	
BSF-1	2.35	3.3	2.4	31.0	5
BSF-2	1.85	5.1	2.9	37.3	6
BSF-3	3.59	16.2	8.1	42.7	6
BSF-3-Co	3.85	12.7	8.5	-	6
BSF-4	2.38	9.8	7.3	35.0	7
JCM-1	3.5	13.7	8.1	36.9	8
TIFSIX-2-Cu-i	4.1	6.5 ^c	55	46.3	9
MUF-17	3.0	6	7.1	49.5	10
UTSA-220	3.4	4.4	10	29.0	11
ZrT-1-tetrazol	2.58	2.8	4.1	33.2	12
ZNU-9	7.94	10.3	11.6	33.1	13
ZNU-1	3.40	56.6	19.7	54.0	14
M ³ MOF-3a	1.87	8.4	5.2	27.1	15
SIFSIX-Cu-TPA	8.26	5.3	15 ^e	39.1	16
sql-SIFSIX-bpe-Zn	1.78	8.4	53.1	67.5	17
FJUT-1	5.94	4.06	4.07	43.7	18
ZJUT-6	4.93	8.9	12.2	35.0	<i>This work</i>

^a Adsorption capacity is obtained from single-component gas adsorption isotherms.

^b Q_{st} values at low surface coverage.

^c At low loading.

^d IAST selectivity for C₂H₂/CO₂ (2/1, v/v) gas mixtures.

^e IAST selectivity for C₂H₂/C₂H₄ (1/1, v/v) gas mixtures.

Supplementary Figures

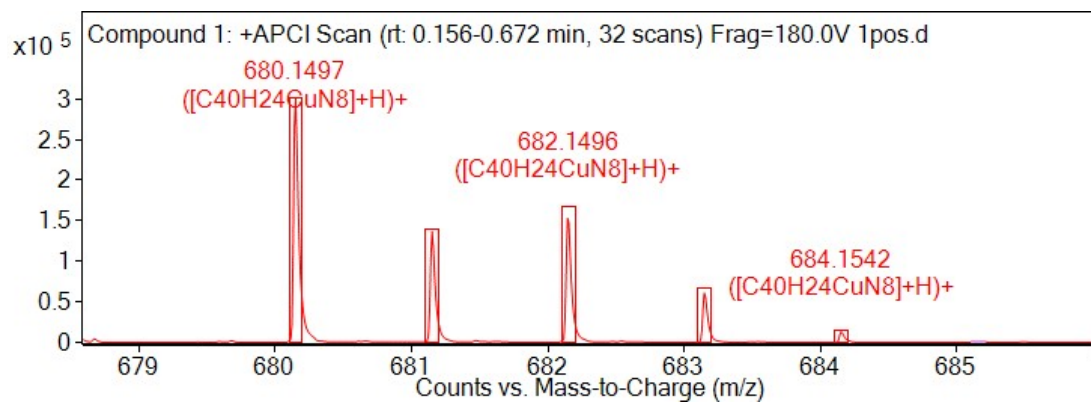


Figure S1. High-resolution mass spectrometry of Cu-TPyP ligand, indicating the successful metallization of TPyP organic linker.

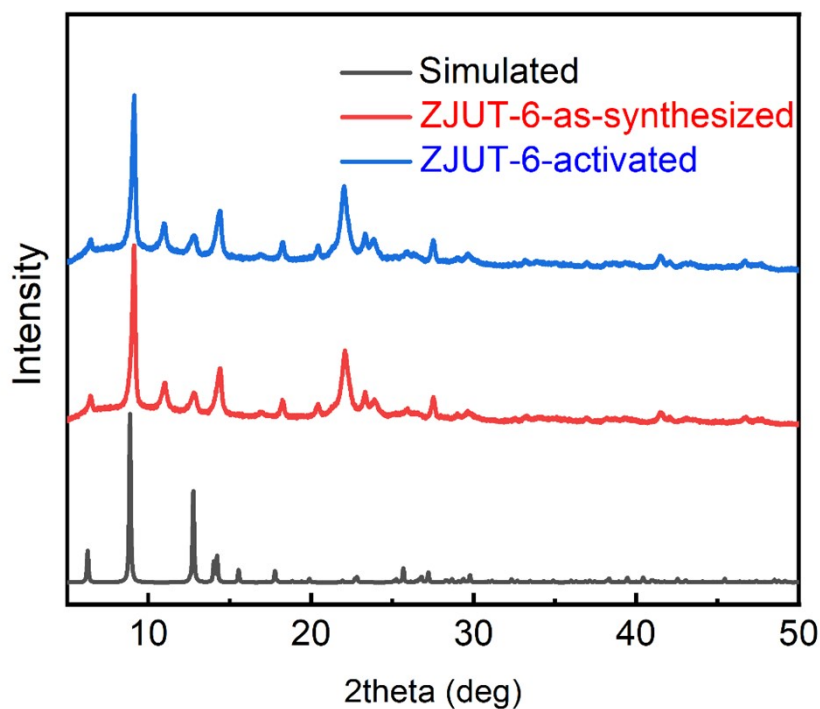


Figure S2. PXRD patterns of as-synthesized ZJUT-6 (red) and active ZJUT-6 (blue) compared with the calculated XRD pattern from the structure of ZJUT-6 (black).

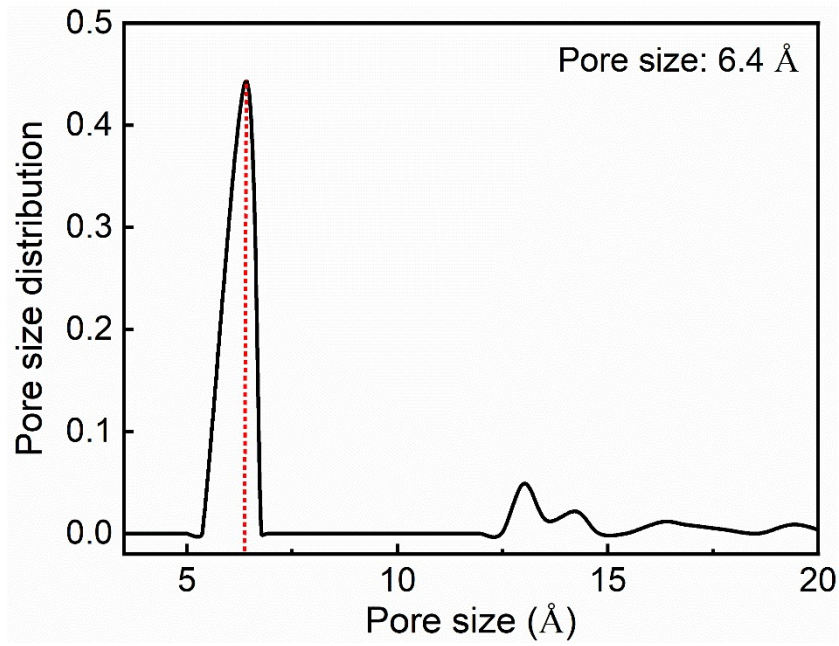


Figure S3. Pore size distribution for ZJUT-6a based on NLDFT model.

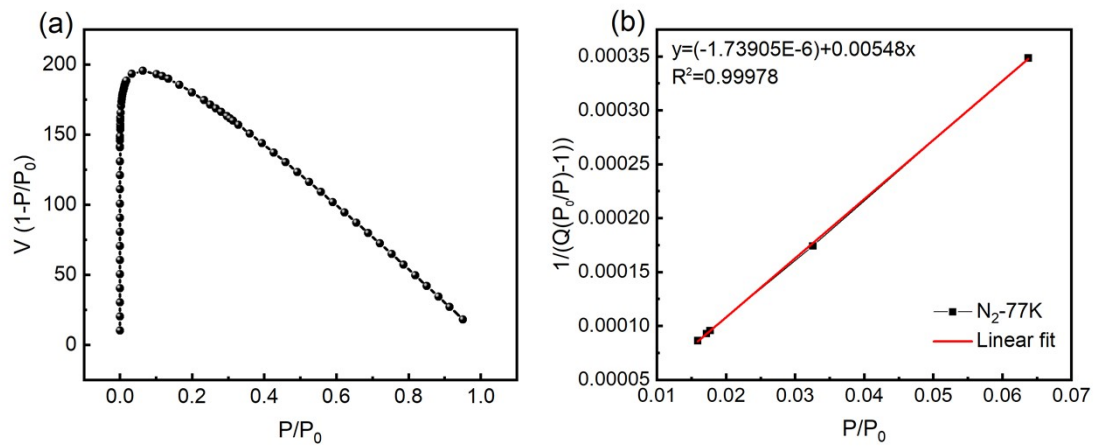


Figure S4. Linear fitting of N_2 sorption isotherms for ZJUT-6a at 77 K.

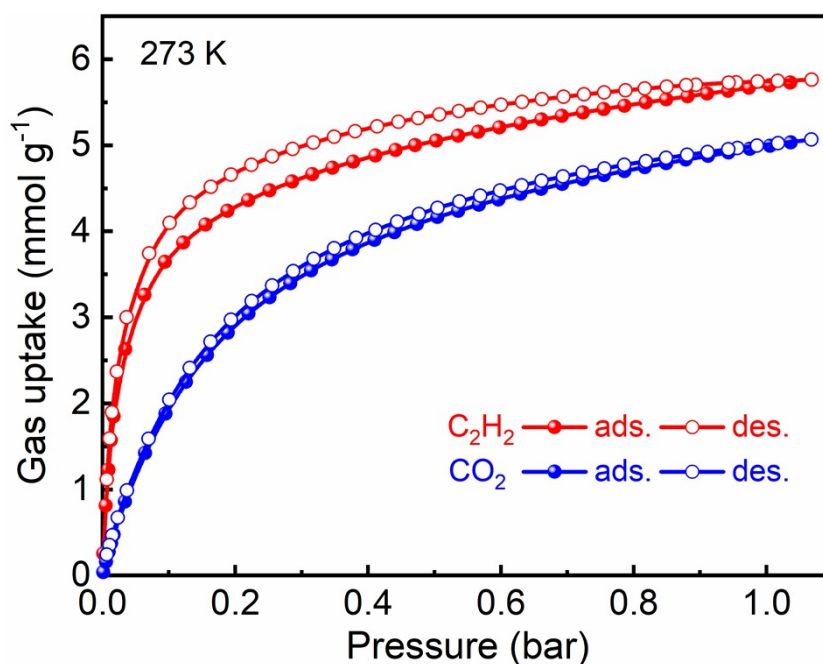


Figure S5. Adsorption isotherms of CO_2 (blue) and C_2H_2 (red) for ZJUT-6a at 273 K up to 1 bar. Filled/empty circles represent adsorption/desorption.

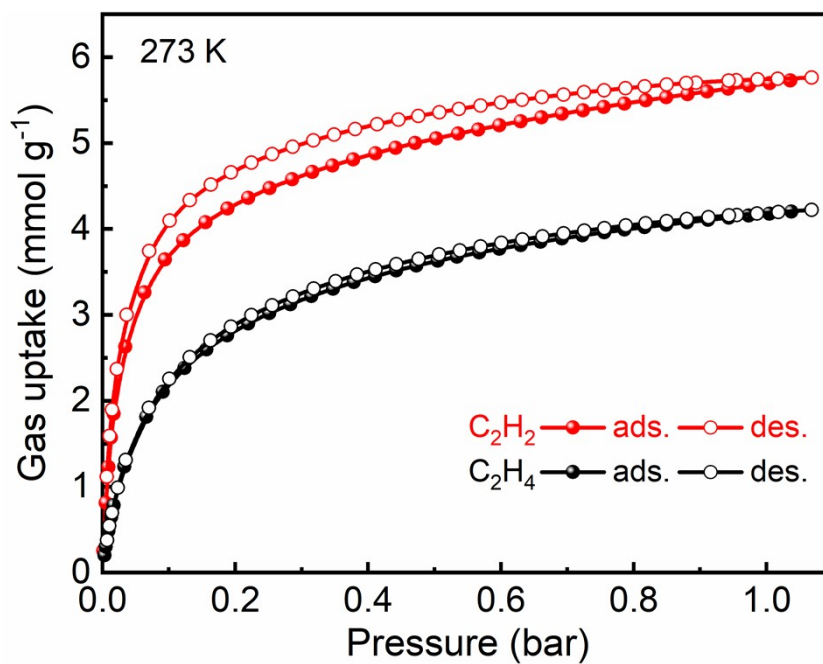


Figure S6. Adsorption isotherms of C_2H_4 (black) and C_2H_2 (red) for ZJUT-6a at 273 K up to 1 bar. Filled/empty circles represent adsorption/desorption.

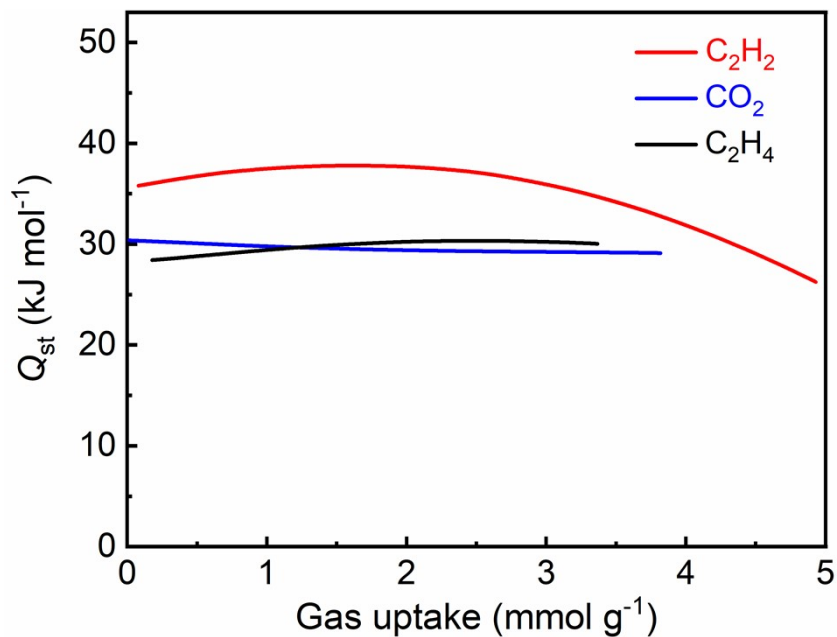


Figure S7. Heat of adsorption (Q_{st}) of C_2H_2 (red), CO_2 (blue) and C_2H_4 (black) for ZJUT-6a.

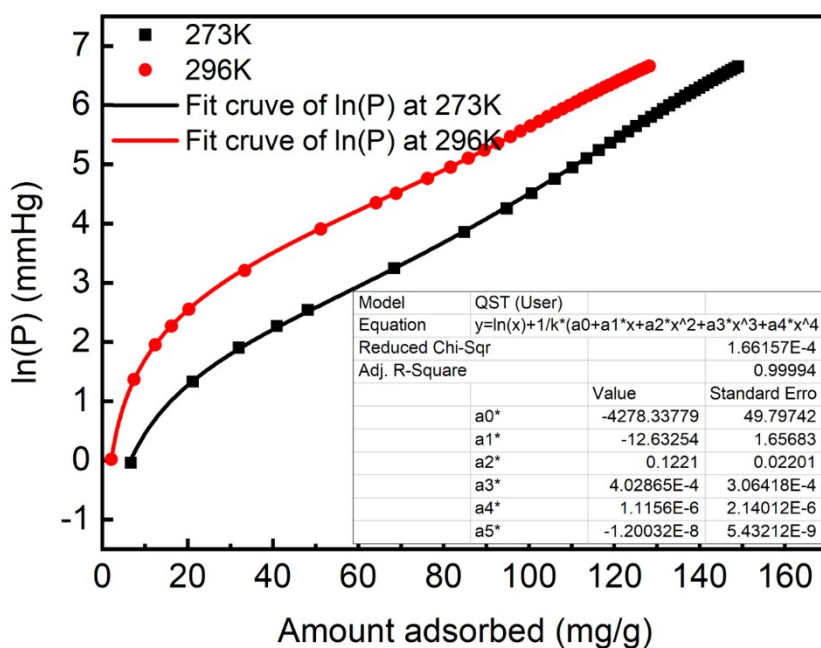


Figure S8. Virial fitting of the C_2H_2 adsorption isotherms for ZJUT-6a.

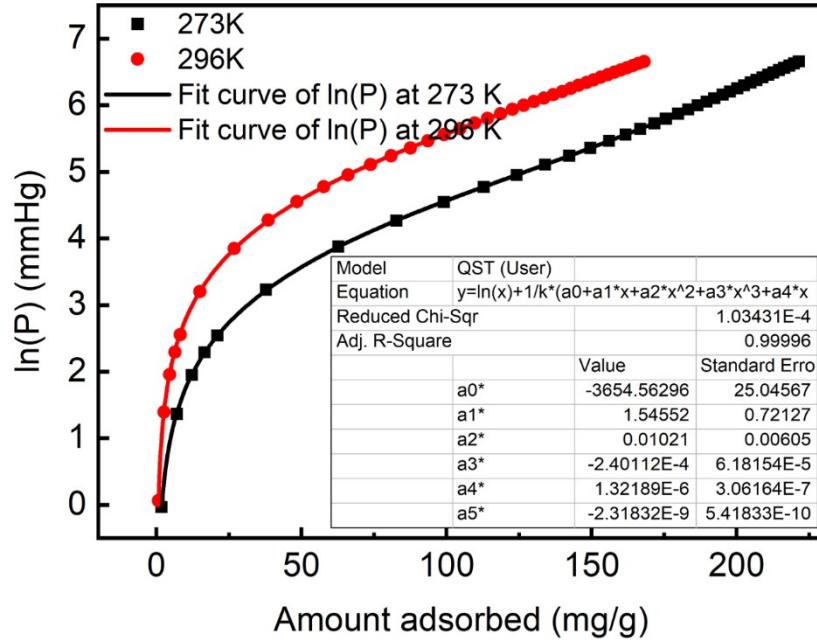


Figure S9. Virial fitting of the CO₂ adsorption isotherms for ZJUT-6a.

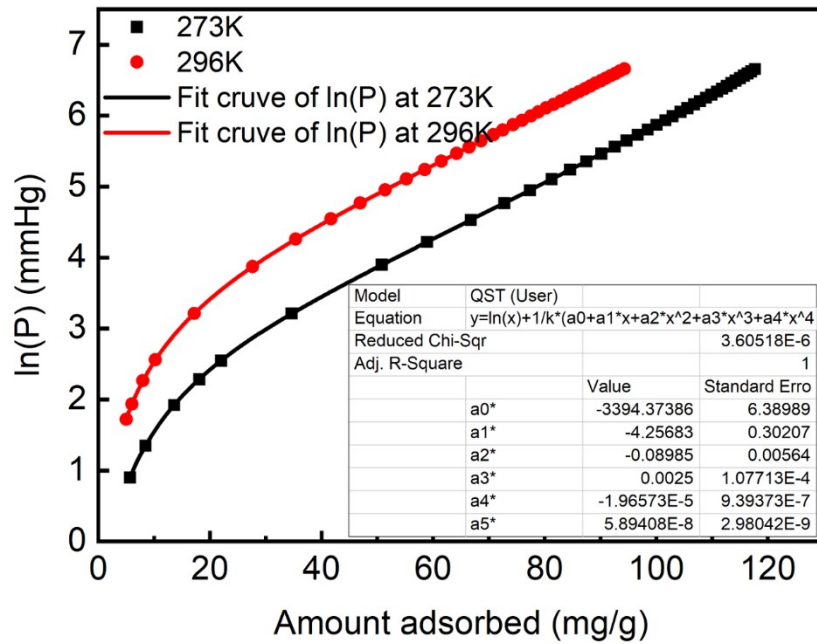


Figure S10. Virial fitting of the C₂H₄ adsorption isotherms for ZJUT-6a.

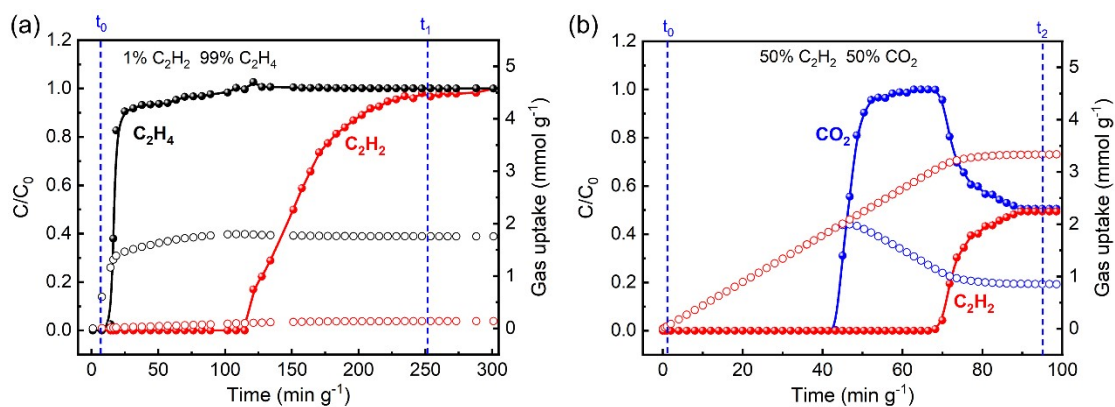


Figure S11. (a) Experimental column breakthrough curves (solid circle) and gas dynamic uptake calculation (hollow Circle) for a 1/99 C_2H_2/C_2H_4 mixture in ZJUT-6a. The calculation of dynamic uptake is based on equation (6). Dashed blue lines: C_2H_2 and C_2H_4 gas adsorbed from t_0 to t_1 (253.8 min g^{-1}) when the C_2H_2 breakthrough was completed. (b) Experimental column breakthrough curves (solid circle) and gas dynamic uptake calculation (hollow Circle) for a 50/50 C_2H_2/CO_2 mixture in ZJUT-6a. Dashed blue lines: C_2H_2 and CO_2 gas adsorbed from t_0 to t_2 (94.6 min g^{-1}) when the C_2H_2 breakthrough was completed.

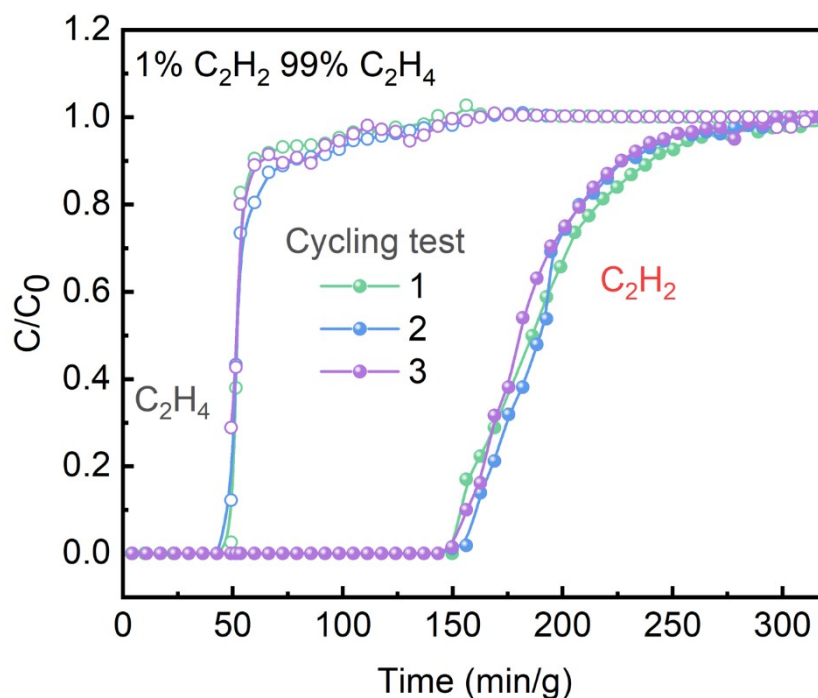


Figure S12. Cycling column breakthrough curves of ZJUT-6a for 1/99 C_2H_2/C_2H_4 mixtures at ambient conditions.

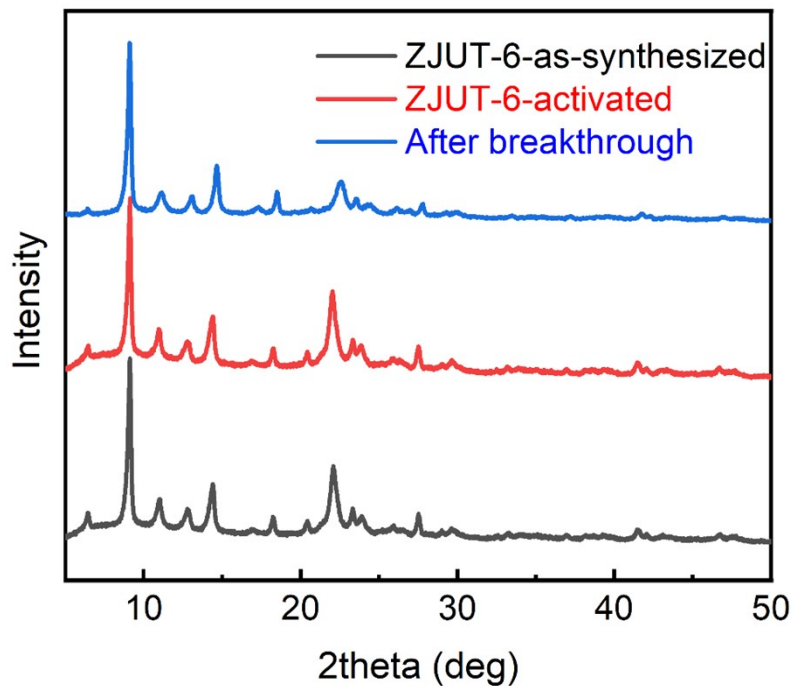


Figure S13. PXRD patterns of as-synthesized ZJUT-6 (black), activated ZJUT-6 (red) and ZJUT-6 samples after multiple breakthrough tests (blue).

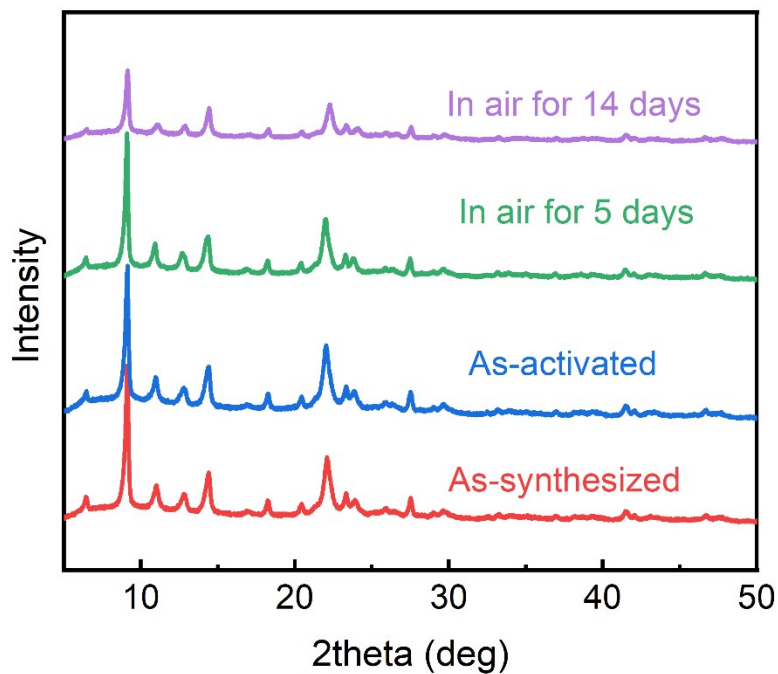


Figure S14. PXRD patterns of Simulated ZJUT-6 (black), as-synthesized ZJUT-6 (red), activated ZJUT-6 (blue), and ZJUT-6 samples exposed to air for 5 days (green), two weeks (purple), indicating its great air stability.

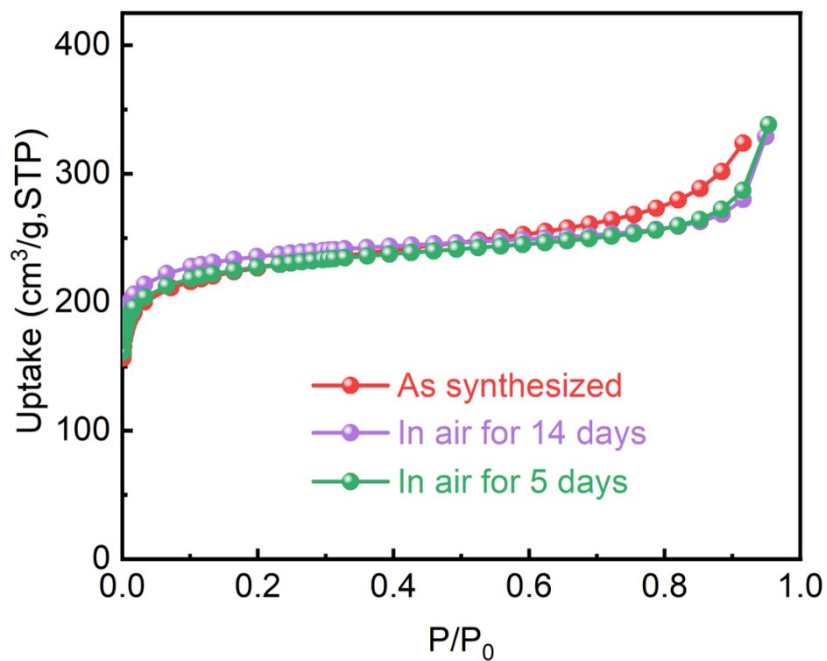


Figure S15. N_2 adsorption isotherms at 77 K of ZJUT-6 samples exposed to air for 5 and 14 days.

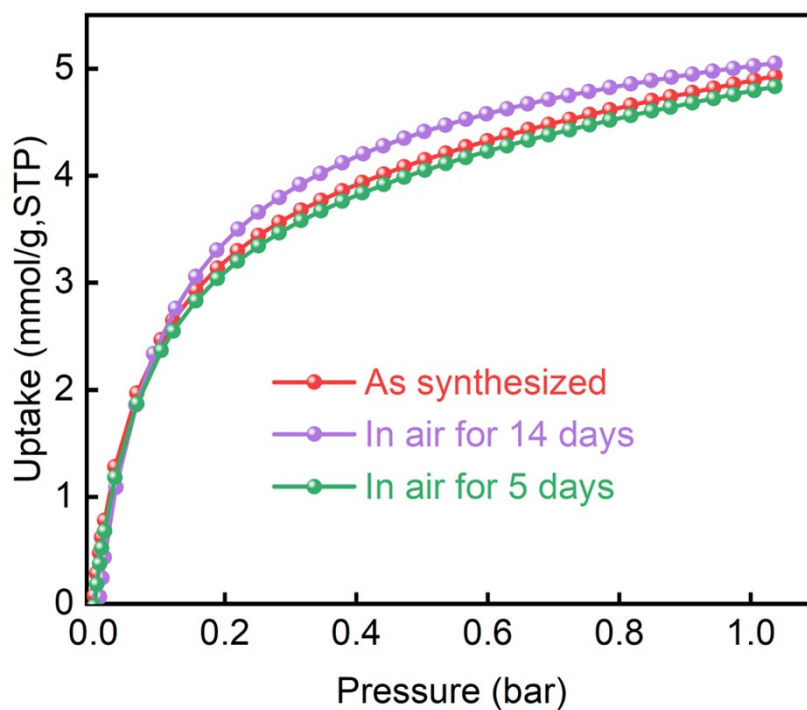


Figure S16. C_2H_2 adsorption isotherms at 296 K of ZJUT-6 samples exposed to air for 5 and 14 days.

Reference

1. W.-H. Zhang, Y.-L. Song, Z.-G. Ren, H.-X. Li, L.-L. Li, Y. Zhang and J.-P. Lang, *Inorg. Chem.*, 2007, **46**, 6647–6660.
2. H.-M. Wen, L. Li, R.-B. Lin, B. Li, B. Hu, W. Zhou, J. Hu and B. Chen, *J. Mater. Chem. A*, 2018, **6**, 6931.
3. (a) Q. Lin, C. Mao, A. Kong, X. Bu, X. Zhao and P. Feng, *J. Mater. Chem. A*, 2017, **5**, 21189; (b) P. Zhang, Y. Zhong, Y. Zhang, Z. Zhu, Y. Liu, Y. Su, J. Chen, S. Chen, Z. Zeng, H. Xing, S. Deng and J. Wang, *Sci. Adv.*, 2022, **8**, eabn9231.
4. X.-W. Gu, J.-X. Wang, E. Wu, H. Wu, W. Zhou, G. Qian, B. Chen and B. Li, *J. Am. Chem. Soc.*, 2022, **144**, 2614.
5. Y. Zhang, L. Yang, L. Wang, S. Duttwyler and H. Xing, *Angew. Chem. Int. Ed.*, 2019, **58**, 8145.
6. Y. Zhang, J. Hu, R. Krishna, L. Wang, L. Yang, X. Cui, S. Duttwyler and H. Xing, *Angew. Chem. Int. Ed.*, 2020, **59**, 17664.
7. Y. Zhang, L. Wang, J. Hu, S. Duttwyler, X. Cui and H. Xing, *Cryst. Eng. Comm*, 2020, **22**, 2649.
8. J. Lee, C. Y. Chuah, J. Kim, Y. Kim, N. Ko, Y. Seo, K. Kim, T. H. Bae and E. Lee, *Angew. Chem. Int. Ed.*, 2018, **130**, 7995.
9. K.-J. Chen, H. S. Scott, D. G. Madden, T. Pham, A. Kumar, A. Bajpai, M. Lusi, K. A. Forrest, B. Space and J. J. Perry, *Chem*, 2016, **1**, 753.
10. O. T. Qazvini, R. Babarao and S. G. Telfer, *Chem. Mater.*, 2019, **31**, 4919.
11. H. Li, L. Li, R.-B. Lin, G. Ramirez, W. Zhou, R. Krishna, Z. Zhang, S. Xiang and B. Chen, *ACS Sustainable Chem. Eng.*, 2019, **7**, 4897.
12. W. Fan, S. B. Peh, Z. Zhang, H. Yuan, Z. Yang, Y. Wang, K. Chai, D. Sun and D. Zhao, *Angew. Chem. Int. Ed.*, 2021, **60**, 17338.
13. Y. Zhang, W. Sun, B. Luan, J. Li, D. Luo, Y. Jiang, L. Wang and B. Chen, *Angew. Chem. Int. Ed.*, 2023, **62**, e202309925.
14. L. Wang, W. Sun, Y. Zhang, N. Xu, R. Krishna, J. Hu, Y. Jiang, Y. He and H. Xing, *Angew. Chem. Int. Ed.*, 2021, **60**, 22865.
15. M. C. Das, Q. Guo, Y. He, J. Kim, C.-G. Zhao, K. Hong, S. Xiang, Z. Zhang, K. M. Thomas, R. Krishna and B. Chen, *J. Am. Chem. Soc.*, 2012, **134**, 8703.
16. H. Li, C. Liu, C. Chen, Z. Di, D. Yuan, J. Pang, W. Wei, M. Wu and M. Hong, *Angew. Chem. Int. Ed.*, 2021, **60**, 7547–7552.
17. M. Shivanna, K.-i. Otake, B.-Q. Song, L. M. van Wyk, Q.-Y. Yang, N. Kumar, W. K. Feldmann, T. Pham, S. Suepaul, B. Space, L. J. Barbour, S. Kitagawa and M. J. Zaworotko, *Angew. Chem. Int. Ed.*, 2021, **60**, 20383–20390.
18. L. Zhang, T. Xiao, X. Zeng, J. You, Z. He, C.-X. Chen, Q. Wang, A. Nafady, A. M. Al-Enizi and S. Ma, *J. Am. Chem. Soc.*, 2024, **146**, 7341–7351.